Quantum Electronics **51** (9) 795–800 (2021)

https://doi.org/10.1070/QEL17611

Generation of electron–positron pairs by laser-ion implosion of a target with a spherical microbubble inside

D.A. Serebryakov, I.Yu. Kostyukov, M. Murakami

Abstract. **Laser targets with microbubbless have recently been intensely studied, including with the aim of generating superintense electromagnetic fields. Under the action of laser radiation, ion beams are formed in the target, converging to the centre of the microbubbles. In the central region, the ion density can be several times higher than the target density, leading to the generation of an extremely intense electric field and high-energy ions. Using PIC simulation, the dynamics of target electrons is investigated taking into account the effects of quantum electrodynamics (QED) and the development of a QED cascade in the intense field region. It is shown that an increase in the electron temperature leads to a much more efficient formation of electron–positron pairs. The contribution of bremsstrahlung to the generation of photons in the central region of the microbubbles is analysed. It is found that the contribution of bremsstrahlung is insignificant in comparison with the synchrotron mechanism of electron emission in the collective field of ions.**

Keywords: *laser pulses, interaction of laser radiation with matter, quantum electrodynamics, electron–positron pairs.*

1. Introduction

Research into extreme states of matter is an important area of modern science, contributing to the advancement of knowledge in atomic and nuclear physics, plasma physics, astrophysics and other sciences. To date, a large number of laser schemes have been implemented and proposed, aimed at achieving extreme states of matter. Most of them are associated with the implementation of inertial controlled thermonuclear fusion [1]. Recently, schemes for the generation of extremely intense electromagnetic (EM) fields have been of great interest, which will make it possible to study, among other things, the nonperturbative effects of quantum electrodynamics (QED) [2] and the formation of a macroscopic amount of matter due to QED cascades [3, 4]. In this regard, attention is drawn to various configurations of the laser field, realised by combining several high-power laser pulses. Among them, worth noting are both the coherent addition of elliptically polarised tightly focused pulses [5, 6], and the generation of a laser 'dipole wave' [7, 8]. This coherent combining allows obtaining a much larger amplitude at the focus of the field than in the case of using a single pulse with a power equal to the total multipulse configuration power.

On the other hand, it has been recently shown that extremely strong fields could be obtained using relativistic electron beams and high-power laser pulses [9, 10]. The main factors allowing this to be achieved are the focusing of the beam to nanometre transverse dimensions (unattainable for optical radiation) and the relativistic increase in the field by several orders of magnitude in the intrinsic reference frame in accordance with the Lorentz transformations. The calculation results show that in this case, in the particle rest frame, it is possible to generate EM fields with an intensity several orders of magnitude higher than that of the critical QED field (Sauter–Schwinger field).

A disadvantage of the methods proposed above is the necessity for using laser radiation and electron beams, the parameters of which significantly exceed those of modern laser facilities and electron accelerators. Recently, a new approach has been proposed that combines the advantages of beam and laser systems and, at the same time, does not require extremely high laser intensities [11, 12]. Calculations show that this scheme can provide the generation of an electric field with an intensity much higher than the intensity of the laser field currently achievable under laboratory conditions. The essence of the proposed approach consists in laser irradiation of a target containing a spherical microbubbles. Hot electrons resulting from the ionisation and heating of the target under action of laser radiation fill a previously almost empty bubble and draw out ions from the target plasma with their charge, causing the appearance of ion fluxes spherically converging in the centre of the microbubbles. In the central region, the ion density can be several times higher than the target density, leading to the generation of an extremely intense electric field and the formation of high-energy ions. In addition to targets with spherical microbubbless, microbubbless with cylindrical geometry were also investigated. Numerical simulation has shown that such configurations can be used to generate superintense magnetic fields [13, 14].

In an intense electric field, the probabilities of QED processes become rather high. Since the electric field strength at the focusing point can significantly exceed the laser field strength achievable under laboratory conditions, the use of laser targets with a spherical microbubbles can be considered a promising method for studying the effects of high-field QED. Estimates show that generation of high-energy photons and electron–positron pairs is possible in this configuration [15, 16]. Of particular interest are QED cascades that have not yet been studied for this EM field configuration and can

D.A. Serebryakov, I.Yu. Kostyukov Institute of Applied Physics, Russian Academy of Sciences, ul. Ulyanova 46, 603950 Nizhny Novgorod, Russia; e-mail: dms@appl.sci-nnov.ru;
M. Murakami Institute of Laser Engineering, Osaka University, 565-0871, Japan

Received 15 May 2021; revision received 9 July 2021
Kvantovaya Elektronika **51** (9) 795–800 (2021)
Translated by V.L. Derbov

affect the focusing of ions in a bubble. QED cascades are multiply repeated time sequences of the following processes: 1) acceleration of charged particles in an EM field; 2) emission of high-energy photons by accelerated particles; and 3) decay of photons in a field into electron–positron pairs. As the cascade develops, the number of electrons, positrons, and photons grows exponentially with time. In this case, the energy for the cascade development is consumed from the EM field, and the resulting electron–positron plasma, in turn, can affect the field distribution.

In Refs [15, 16], QED processes were analysed with the participation of external particles, and the analysis itself was limited to the simplest estimates. In this work, we investigate possible QED processes in a spherical microbubbles under more realistic conditions (in particular, taking into account the temperature of plasma electrons, which is determined by the parameters of laser radiation incident on the target), without attracting external particles. For this purpose, numerical simulation based on the particle-in-cell (PIC) method is used to describe plasma processes and the Monte Carlo method is employed to describe QED effects.

2. Electron dynamics and QED processes in a microbubbles

For numerical simulation, we used the three-dimensional QED-PIC code QUILL [17, 18]. In this work, we confined ourselves to the non-self-consistent problem, in which the ions were described by specifying the external field in the code. Self-consistent simulation of laser implosion of a target, as well as the dynamics of ions and electrons, without taking into account QED effects, was carried out in Ref. [11]. In our case, the dynamics of the target electrons was numerically simulated (under the action of the field of ions, most of which are concentrated in the central region of the microbubbles, the electrons move to the centre of the microbubbles), as well as the emission of photons by electrons and positrons in a given ion field and the decay of these photons into electron–positron pairs. The ion field used in the simulation was approximately calculated in [12]:

$$E_{\mathrm{f}}(r) = 4E_{\max}\left(\frac{r_{\min}}{r} - \frac{r_{\min}^2}{r^2}\right), \qquad (1)$$

where $E_{\max}$ is the maximum field amplitude (attained at $r = 2r_{\min}$), and $r_{\min}$ is the radius at which the collapse of the inner ionic shell stops [11]. The following parameters were used in the calculations: $R_0 = 1$ μm is the radius of the microbubbles, $r_{\min} = 1$ nm, and the $E_{\max}$ value was in the range 10000–25000. The field strength is specified in dimensionless units and normalised to $2\pi mc^2/(\lambda e)$, where c is the speed of light; e and m are the electron charge and mass, respectively; and $\lambda = 1$ μm is the laser wavelength.

The time dependence of the field was absent in some of the numerical calculations (the field was stationary), and in a part of the calculations, the process of smooth on/off switching of the field during time σ_{t} was modelled: $E(r,t) = E(r)(1 + (t - t_0)^2/\sigma_{\mathrm{t}}^2)$. The dependence of the field on the radial coordinate and time was set on a grid (in the form of a 2D array of the required accuracy), and the external field at specific points in space was calculated by linear interpolation of the elements of this array. Figure 1 shows the profile of the external field calculated using Eqn (1) for typical values of the parameters $E_{\max} = 25000$ and $r_{\min} = 1$ nm.

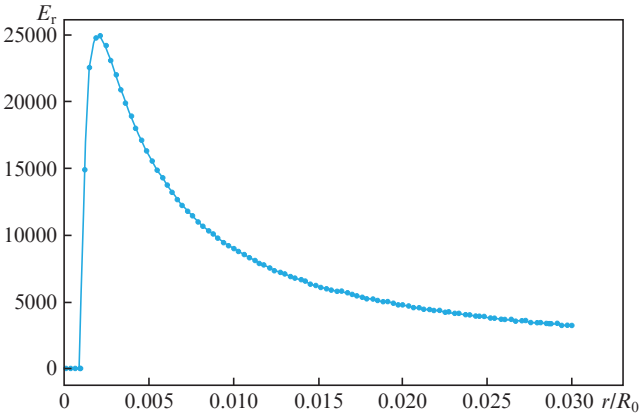

Figure 1. Profile of the external electric field $E_{\mathrm{r}}(r)$, which simulates the field of the central ion bunch, for the parameters $E_{\max} = 25000$ and $r_{\min} = 1$ nm.

The electron cloud in the numerical simulation was set in the form of a uniform-density ball with the centre coinciding with that of the field profile. The electrons initially have a quasi-Boltzmann velocity distribution with a certain temperature T. The ball radius $r_{\max}$ was set large enough to satisfy two criteria. First, it must be much larger than the field scale $r_{\min}$. Second, during the simulation, electrons from the outer regions of the ball should not have time to approach the centre during their collapse (the velocity of electrons approaching the centre being limited by the speed of light). These conditions allow an approximate description of the situation arising in a real problem, when an ion bunch arises in a bubble filled with a hot electron gas with an almost uniform density. The simulation time was chosen equal to $0.03R_0/c \approx 90$ as. This corresponds to the estimates of the compression time of the ion bunch obtained for similar parameters in Ref. [16].

Several series of numerical experiments were carried out. The first simulation was carried out for the parameters $E_{\max} = 15000$, $T = 0$, $r_{\max} = 0.01R_0$, the initial electron density $n_{\mathrm{e}0} = 10n_0 = 1.1 \times 10^{22}$ cm^{-3} (n_0 is the density used for normalisation in PIC codes). In general, they correspond to the parameters used in the simulation [12] performed by the molecular dynamics method (only the electron density differs; however, simulation with different values of the densities did not give noticeable differences in the results). Figure 2 shows the change in the electron density over time. The initial colour used for the electron density corresponded to the level of 1.1×10^{22} cm^{-3}, so that its distribution profile in the outer layers was noticeable. One can see how the electron cloud is compressed under the action of the central field. A specific feature is the formation of spherical structures, which is a consequence of oscillations of electrons relative to the centre. Since at zero initial temperature the electron velocity always has only a radial component, the outer layer of electrons collapses spherically symmetrically to the centre; then the electrons fly through the central region by inertia, and collapsing and expanding spherical shells are observed at certain times.

Figure 3 shows the change in the electron density profile for the same numerical calculation. At the centre, the density exceeds 3×10^{23} cm^{-3}, but its growth stops after $t = 0.06\lambda/c$, since by this time all electrons from the outer layers reach the centre. This means that the radius of the electron ball $r_{\max} =$

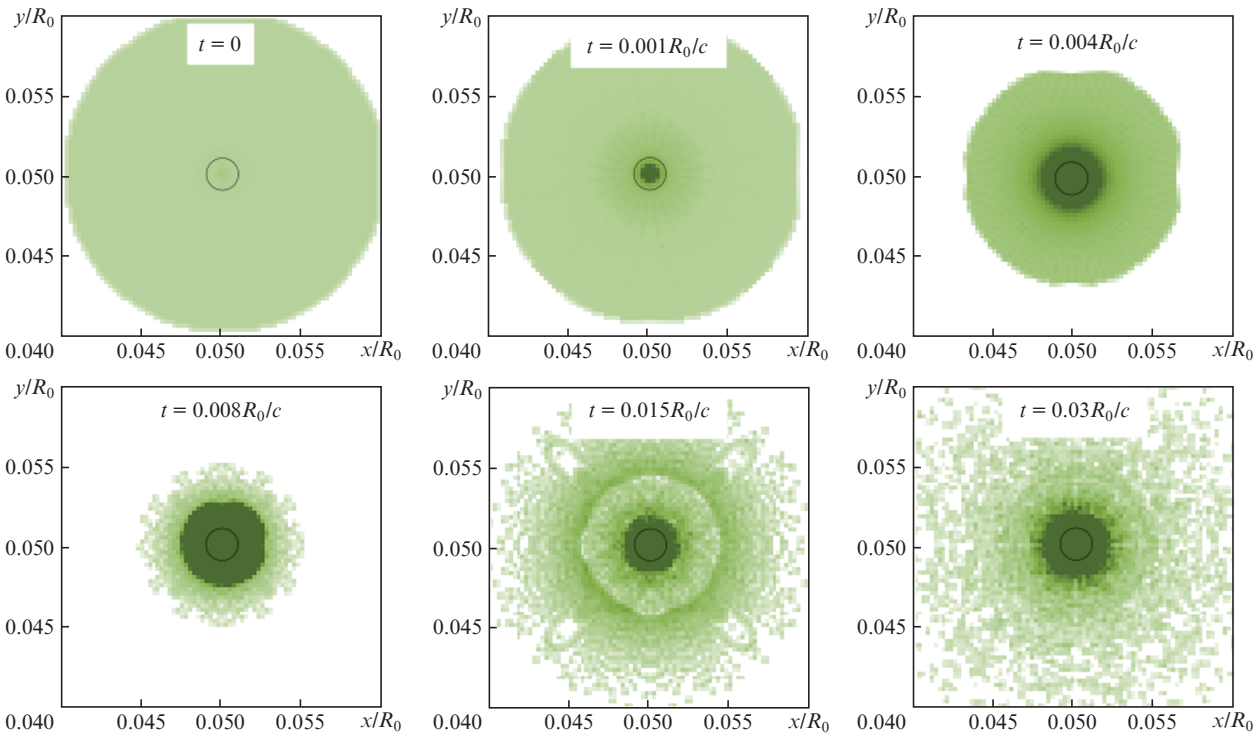

Figure 2. (Colour online) Electron density distributions in PIC simulations at different times for a 'small' electron cloud ($r_{max} = 0.01R_0$) and zero initial electron temperature in the case of a stationary external field. The black circle shows the characteristic size of the external field with $r_{min} = 0.001R_0$.

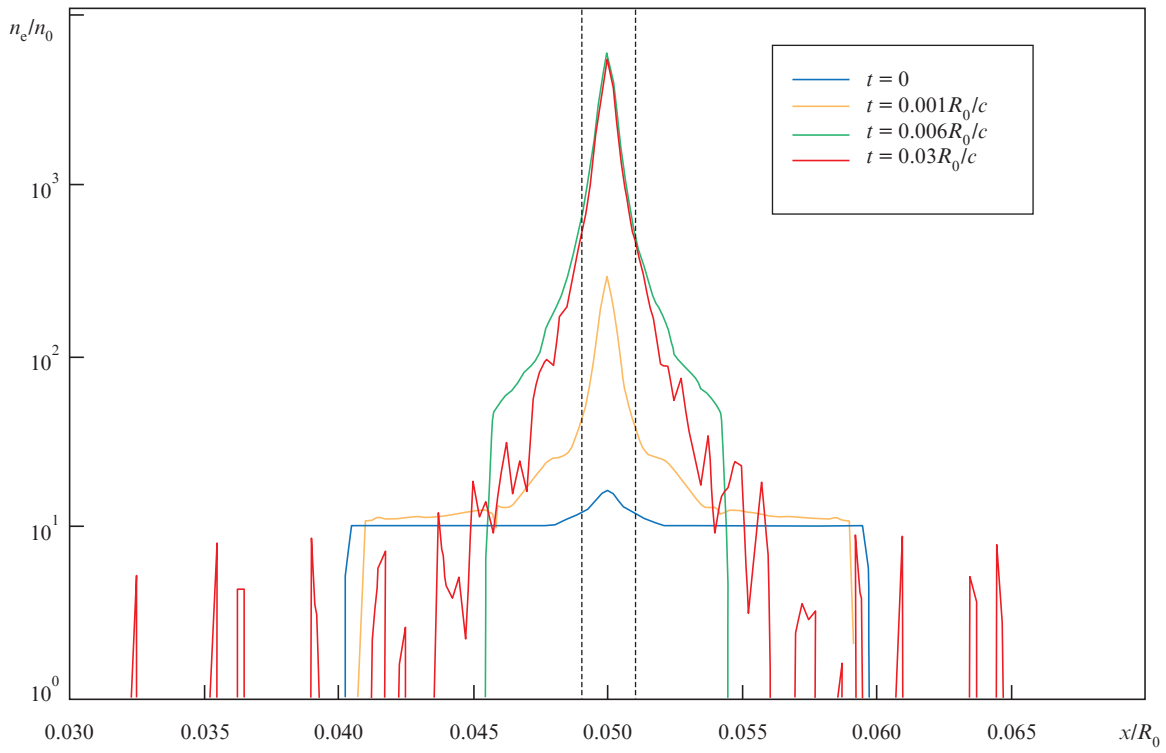

Figure 3. (Colour online) Electron density profiles in PIC simulations at different times for a 'small' electron cloud (simulation parameters are the same as in Fig. 1). The vertical dashed lines show the characteristic size of the external field with $r_{min} = 0.001R_0$.

$0.01\,R_0$ is insufficient for correct simulation of the collapse of the electron cloud, but it allows qualitative tracking of the collapse process.

Next, a numerical simulation was performed for an electron cloud with $r_{max} = 0.08\,R_0$, with the initial electron temperature $T = 10$ MeV, the other parameters being unchanged.

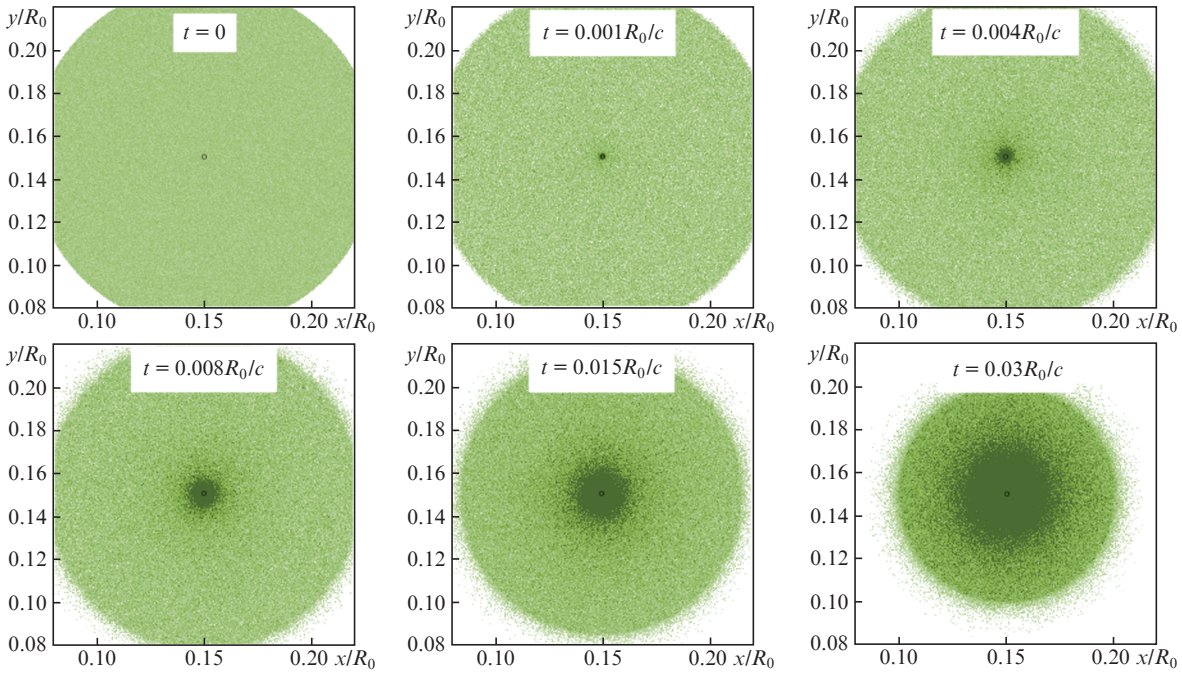

Figure 4. (Colour online) Electron density distributions in PIC simulations at different times for a 'large' electron cloud ($r_{max} = 0.08R_0$) and electron temperature $T = 10$ MeV in the case of a stationary external field. The black circle shows the characteristic size of the external field with $r_{min} = 0.001R_0$.

The collapse process for these parameters is shown in Figs 4 and 5. When crossing the region of an intense EM field, electrons can emit photons, which at the considered field amplitude can lead to photon decay with the formation of an electron–positron pair and the development of a QED cascade. The development of the cascade can be seen in Fig. 6, which shows the time dependences of the energies of positrons and hard radiation photons. In the calculations, the initial tem-

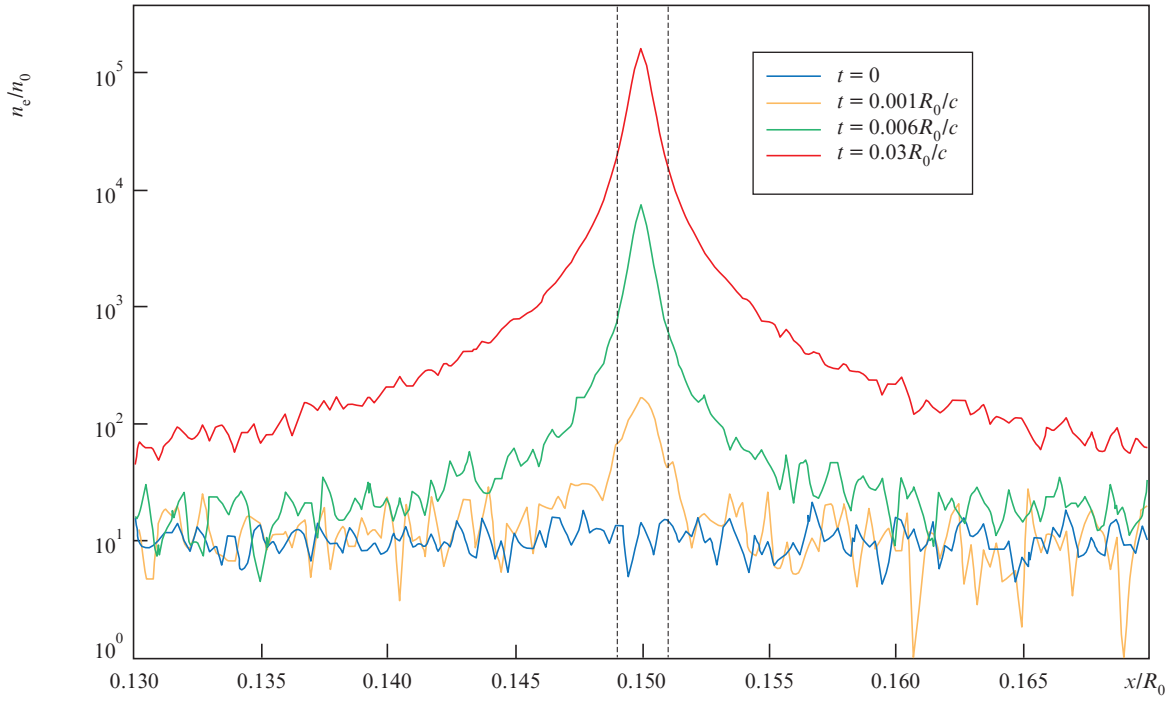

Figure 5. (Colour online) Electron density profiles in PIC simulations at different points in time for a 'large' electron cloud. The vertical dashed lines show the characteristic size of the external field, $r_{min} = 0.001R_0$.

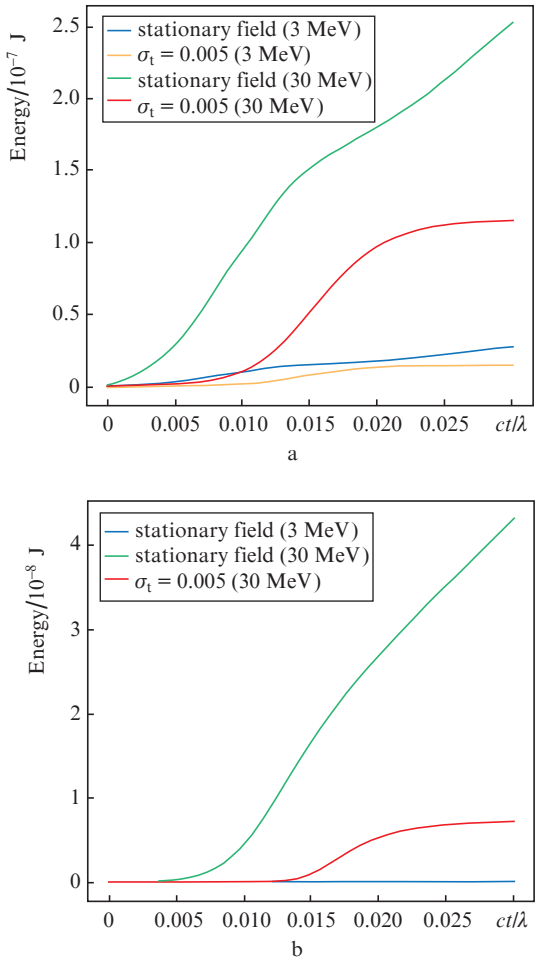

Figure 6. (Colour online) Numerical simulation of the time dependence of the energy of (a) photons and (b) positrons at the initial temperature T = 3 and 30 MeV for stationary and nonstationary (σ_t = 0.005) fields; E_{max} = 15000.

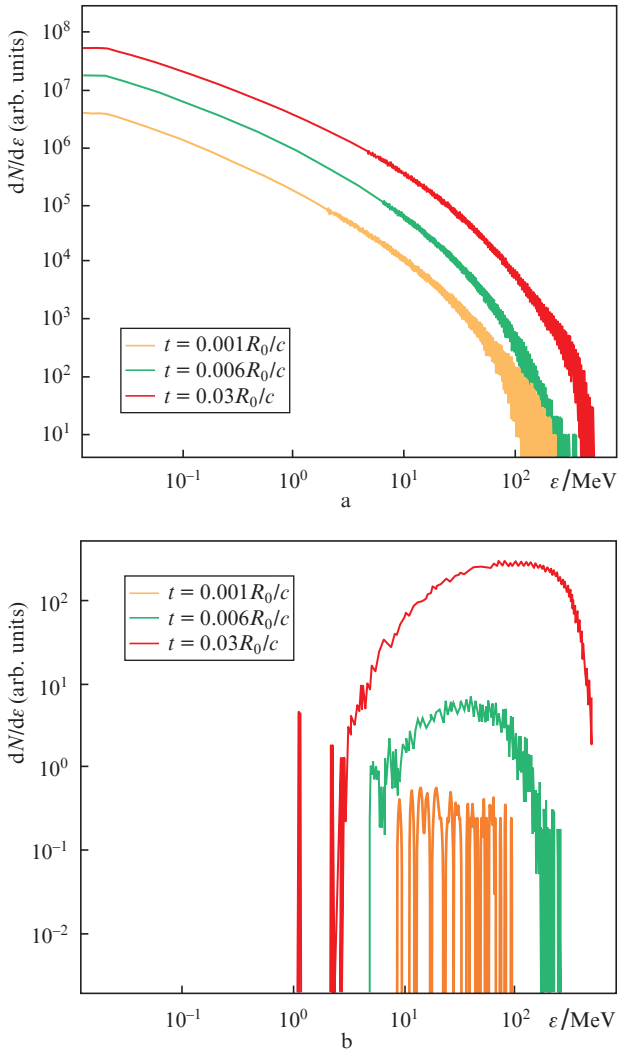

Figure 7. (Colour online) Energy spectra of (a) photons and (b) positrons at different times for the same parameters of numerical simulation as in Figs 3 and 4.

perature of the electron cloud was varied. The main regularity is that an increase in the initial temperature leads to a much faster development of the cascade. Moreover, as follows from the calculation results, at zero temperature the cascade virtually does not develop at the same field amplitude. This effect is expected, since the probability of QED processes increases with increasing transverse field strength (with respect to the particle trajectory). If the initial temperature in the calculations is equal to zero, the electrons move exclusively along the radial coordinate and the radial field acts on them (that is, there is no transverse field component). Therefore, QED processes are strongly suppressed.

In addition, it can be seen from Fig. 6, that in the case of a nonstationary field (at the initial moment of time the field is weak, then it increases to a maximum, followed by a decrease), a similar dependence of QED processes on the initial temperature of electrons is observed, but the total energy of the produced photons and pairs turns out to be several times lower. Figure 7 shows the spectra of photons and positrons for the simulation parameters $r_{max} = 0.08R_0$, T = 10 MeV. An increase in the maximum energy of photons and positrons with time is noticeable, which corresponds to the development of a cascade. The positron spectra also show an increase in the average positron energy with time. As the simulation results show, for the parameters under study, the emerging electron–positron plasma practically does not affect the field distribution.

3. Estimation of the bremsstrahlung contribution

The used numerical approach considers the emission of photons in an intense centrally symmetric field of an ion bunch with further formation of electron–positron pairs and the development of a QED cascade. However, when electrons collide with individual ions located in the central region, bremsstrahlung photons are also emitted. It makes sense to compare the number of photons that can be produced in accordance with each of the mechanisms. The characteristic number of produced photons can be estimated by the formula for the bremsstrahlung cross section in the ultrarelativistic limit, using the Coulomb potential approximation without screening [19]:

$$\sigma_b = 4Z^2 \alpha r_e^2 \left(\ln 2\gamma - \frac{1}{3}\right), \qquad (2)$$

where γ is the relativistic Lorentz factor for electrons (for estimation, the characteristic value in numerical calculations can be taken γ = 20); Z is the charge number of the nucleus; r_e is

the classical radius of an electron; and $\alpha \approx 1/137$ is the fine structure constant. The simulation was carried out for hydrogen ions; therefore, $Z = 1$. Then $\sigma_b \approx 8.51 \times 10^{-27}$ cm^2. It should be noted that for relativistic electrons the scattering cross section depends rather weakly on the parameters (electron energy, specific screening of the potential), and the estimates of σ_b obtained using other approximations coincide in order of magnitude with the above.

The number of photons emitted from a unit volume of an electron gas is defined as

$$n_{b\,ph}(r) \approx n_e(r) n_i(r) c\tau\sigma_b, \tag{3}$$

where n_e and n_i are the densities of electrons and ions in a given unit volume; τ is the time during which the number of emitted particles is counted (in the context of the problem, it can be estimated from above as the simulation time of the order of $10 r_{min}/c$). The density of ions is calculated as [11]

$$n_i(r) \approx \frac{1}{6} n_{e0} \left(\frac{r^2}{R_0}\right)^{-2}. \tag{4}$$

Thus, the total number of emitted photons is

$$N_{b\,ph} \approx \int_0^{R_0} n_e(r) n_i(r) c\tau\sigma_b 4\pi r^2 \mathrm{d}r, \tag{5}$$

$$N_{b\,ph} \approx \frac{2}{3}\pi c\tau\sigma_b n_{e0} R_0^2 \int_0^{R_0} n_e(r)\mathrm{d}r. \tag{6}$$

The last integral can be calculated numerically using the electron density distribution found in numerical experiments. For estimate, the distribution shown in Fig. 4 (at the final moment of time) was taken. For the considered parameters, the integral of this distribution is $20.7 R_0 n_0$ or $20.7 R_0 1.1 \times 10^{21}$ cm^{-3}. The unperturbed electron density is $n_{e0} = 10 n_0 = 1.1 \times 10^{22}$ cm^{-3}. If we use $R_0 = 1$ μm and $r_{min} = 1$ nm for the estimate, then substituting these values of the parameters, we obtain

$$N_{b\,ph} \approx \frac{2}{3}\pi 10 r_{min} 8.51 \times 10^{-27} \times n_{e0} 20.7 R_0^3 1.1 \times 10^{21} \approx 4.47. \tag{7}$$

Thus, during the simulation, the effective number of emitted bremsstrahlung photons is below 5, which is several orders of magnitude smaller than the number of photons produced directly in the collective field of ions due to the synchrotron mechanism. According to the simulation results, it was 1.26×10^5 for these parameters. The above estimate allows us to conclude that bremsstrahlung does not play a key role in the problem under consideration (for the used values of the parameters); therefore, simulation of the emission of photons directly in an external (collective) field without taking into account the bremsstrahlung arising from the scattering of electrons by individual ions is quite justified.

4. Conclusions

Three-dimensional numerical simulation by the particle-in-cell method and the Monte Carlo method allowed the dynamics of hot electrons inside a microbubbles to be studied with QED processes taken into account. As a result of the interaction of laser radiation with a target containing a spherical microbubbles, hot electrons fill the microbubbles and draw target ions into the microbubbles. The ions moving towards the centre of the target form a large charge and an intense EM field in the central region. We have investigated the electron dynamics with allowance for QED processes at the stage when the ion field strength reaches its maximum. In this case, the probability of QED processes becomes significant.

It is shown that with an increase in the electron temperature, both the number of high-energy photons and the number of electron–positron pairs formed increase because of the decay of such photons. As the temperature rises, the energy of secondary particles also increases. The contribution of bremsstrahlung is insignificant in comparison with the synchrotron mechanism of electron emission in the collective field of ions. For the parameters under study, the emerging electron–positron plasma practically does not affect the distribution of the ion field.

Electronic dynamics and QED processes were modelled within the framework of a non-self-consistent approach, when the ion field was specified, rather than calculated, taking into account the ion dynamics. A short time interval was also considered, corresponding to the maximum values of the EM field strength inside the microbubbles. This approach seems to be justified for a detailed study of QED processes with a high spatiotemporal resolution. In the future, it is planned to switch to simulating a complete self-consistent problem taking into account QED processes, with the calculation of laser heating of the target and the dynamics of electrons and ions.

Acknowledgements. This work was supported by the Russian Foundation for Basic Research and the Japan Society for the Promotion of Science (JSPS) (Research Project No. 20-52-50013) and the Ministry of Science and Higher Education of the Russian Federation (State Assignment of the IAP RAS, Project No. 0035-2019-0012).

References

1. Betti R., Hurricane O.A. *Nat. Phys.*, **12** (5), 435 (2016).
2. Fedotov A. *J. Phys. Conf. Ser.*, **826**, 012027 (2017).
3. Nerush E.N., Kostyukov I.Yu. *Phys. Rev. E*, **75** (5), 057401 (2007).
4. Nerush E.N., Kostyukov I.Yu., Fedotov A.M., Narozhny N.B., Elkina N.V., Ruhl H. *Phys. Rev. Lett.*, **106** (3), 035001 (2011).
5. Bulanov S.S., Mur V.D., Narozhny N.B., Nees J., Popov V.S. *Phys. Rev. Lett.*, **104** (22), 220404 (2010).
6. Gelfer E.G., Mironov A.A., Fedotov A.M., Bashmakov V.F., Nerush E.N., Kostyukov I.Yu., Narozhny N.B. *Phys. Rev. A*, **92** (2), 022113 (2015).
7. Gonoskov A.A., Gonoskov I.A., Harvey C., Ilderton A., Kim A.V., Marklund M., Mourou G., Sergeev A.M. *Phys. Rev. Lett.*, **111** (6), 060404 (2013).
8. Magnusson J., Gonoskov A.A., Marklund M., Esirkepov T.Zh., Koga J.K., Kondo K., Kando M., Bulanov S.V., Korn G., Bulanov S.S. *Phys. Rev. Lett.*, **122** (25), 254801 (2019).
9. Yakimenko V., Meuren S., Del Gaudio F., Baumann C., Fedotov A.M., Fiuza F., Grismayer T., Hogan M.J., Pukhov A., Silva L.O., et al. *Phys. Rev. Lett.*, **122** (19), 190404 (2019).
10. Baumann C., Nerush E.N., Pukhov A., Kostyukov I.Yu. *Sci. Rep.*, **9** (1), 1 (2019).
11. Murakami M., Arefiev A., Zosa M.A. *Sci. Rep.*, **8** (1), 1 (2018).
12. Murakami M., Arefiev A., Zosa M.A., Koga J.K., Nakamiya Y. *Phys. Plasmas*, **26** (4), 043112 (2019).
13. Murakami M., Honrubia J.J., Weichman K., Arefiev A.V., Bulanov S.V. *Sci. Rep.*, **10** (1), 1 (2020).
14. Weichman K., Murakami M., Robinson A.P.L., Arefiev A.V. *Appl. Phys. Lett.*, **117** (24), 244101 (2020).
15. Koga J.K., Murakami M., Arefiev A.V., Nakamiya Y. *Matter and Radiation at Extremes*, **4** (3), 034401 (2019).
16. Koga J.K., Murakami M., Arefiev A.V., Nakamiya Y., Bulanov S.S., Bulanov S.V. *Phys. Lett. A*, **384** (34), 126854 (2020).
17. https://ipfran.ru/institute/structure/421969/quill-3d-code.
18. Nerush E.N., Kostyukov I.Yu. *Vopr. At. Nauki Tekh.*, **68** (4), 3 (2010).
19. Koch H.W., Motz J.W. *Rev. Mod. Phys.*, **31** (4), 920 (1959).